

# Evaluation of the contribution of new particle formation to cloud droplet number concentration in urban atmosphere

Sihui Jiang<sup>1</sup>, Fang Zhang<sup>1\*</sup>, Jingye Ren<sup>1</sup>, Lu Chen<sup>1</sup>, Xing Yan<sup>1</sup>, Jieyao Liu<sup>1</sup>, Yele Sun<sup>2</sup>,  
Zhanqing Li<sup>3</sup>

5 <sup>1</sup>College of Global Change and Earth System Science, Beijing Normal University, Beijing 100875, China

<sup>2</sup>State Key Laboratory of Atmospheric Boundary Layer Physics and Atmospheric Chemistry, Institute of Atmospheric Physics, Chinese Academy of Sciences, Beijing, China

<sup>3</sup>Earth System Science Interdisciplinary Center and Department of Atmospheric and Oceanic Science, University of Maryland, College Park, Maryland, USA

10 Correspondence to: F. Zhang, [fang.zhang@bnu.edu.cn](mailto:fang.zhang@bnu.edu.cn);

## Abstract

The new particle formation (NPF) effect on cloud condensation nuclei (CCN) varies widely in diverse environment. The CCN or cloud droplet from NPF sources remains highly uncertain in urban atmosphere which are greatly affected by the high background aerosols and frequent local emissions. In this study, we quantified the NPF effect on cloud droplet number concentration (CDNC, or  $N_d$ ) at typical updraft velocities ( $V$ ) in clouds based on field observations on May 25-June 18, 2017 in urban Beijing. We show that the NPF increases the  $N_d$  by 32-40% at  $V=0.3-3\text{ m s}^{-1}$  during the studied period. The  $N_d$  is reduced by  $11.8\pm 5.0\%$  at  $V=3\text{ m s}^{-1}$  and  $19.0\pm 4.5\%$  at  $V=0.3\text{ m s}^{-1}$  compared to that calculated from constant supersaturations due to the water vapor competition effect, which suppress the cloud droplet formation by decreasing the environmental maximum supersaturation ( $S_{max}$ ). The effect of water vapor competition becomes smaller at larger  $V$  that can provide more sufficient water vapor. However, under extremely high aerosol particle number concentrations, the effect of water vapor competition becomes more pronounced. As a result, although a larger increase of CCN-size particles by NPF event is derived on clean NPF day when the number concentration of pre-existing background aerosol particles is very low, no large discrepancy is presented in the enhancement of  $N_d$  by NPF between the clean and polluted NPF day. We finally reveal a considerable impact of the primary sources on the evaluation of the NPF contribution to  $N_{CCN}$  and  $N_d$  based on a case study. Our study highlights the importance of fully consideration of both the environmental meteorological conditions and multiple sources (i.e. secondary and primary) to evaluate the NPF effect on clouds and the associated climate effects in polluted regions.

15  
20  
25

## 1 Introduction

In the global climate system, aerosols, cloud condensation nuclei (CCN) and cloud droplets are very important components. Clouds, serving as a bridge connecting aerosols and climate, are the most uncertain factor of climate change (IPCC, 2013; Seinfeld et al., 2016; Cai et al., 2020). The microphysical link between aerosols and clouds as the most important part has received extensive attention. Cloud droplet activation is a key process from aerosol to clouds, and researchers have tried to simulate the microphysical processes by using numerical activation models (e.g. Boucher and Lohmann, 1995; Abdul-Razzak et al., 1998; Ghan et al., 1993; Khvorostyanov and Curry, 1999; Abdul-Razzak and Ghan., 2000; Nenes et al., 2001, 2003; Petters et al., 2007; Ren et al., 2018; Genz et al., 2020).

New particle formation events (NPF) have been observed and occurred frequently in different atmospheric environments in the world (Spracklen et al., 2010; Yue et al., 2011; Peng et al., 2017; Kerminen et al., 2018; Bousiotis et al., 2019; Zimmerman et al., 2020). The NPF events was one of the most significant sources of fine particles in the atmosphere (Shi et al., 1999; Stanier et al., 2004; Kulmala and Kerminen, 2008). For example, it has been found that the NPF contributed about 76% of the total fine particle number concentrations in urban Beijing (Wu et al., 2011). These nucleated particles subsequently grow through coagulation or condensation processes to CCN-relevant sizes, or act as CCN in convective clouds (Fan et al., 2013; Li et al., 2010). In reality, the field studies have shown that these fine particles produced from NPF can subsequently turn into an enhancement in  $N_{CCN}$  at cloud-relevant supersaturation (Kalkavouras et al., 2017; Peng et al., 2014; Wu et al., 2015; Ma et al., 2016; Li et al., 2017; Zhang et al., 2019). It was estimated that up to 80% of CCN number concentration ( $N_{CCN}$ ) is from the nucleation process in urban Beijing (Wiedensohler et al., 2008).

However, the  $N_{CCN}$  only reflects the cloud forming potential of aerosol particles at a given supersaturation. The measurement of CCN is usually carried out at constant supersaturations. Different from the prescribed supersaturation used in the evaluation of  $N_{CCN}$ , when calculating the cloud droplet number concentration (CDNC, or  $N_d$ ), researchers considered the dynamic situations in clouds. In clouds, the supersaturation exhibits variable levels that instantaneously adjust to the intensity of cloud updrafts and the particle number size distribution (PNSD) (Nenes et al., 2003; Hudson et al., 2015). So the CDNC, (or  $N_d$ ) depends on the size distribution, chemical properties of aerosol and the cloud updraft velocity, all of which regulate the maximum supersaturation ( $S_{max}$ ) that can be formed in a cloud parcel (Nenes and Seinfeld, 2003). Studies have shown that the CDNC in clouds exhibits a sublinear relationship to aerosol number concentration ( $N_{CN}$ ) (Twomey, 1977; Leaitch et al., 1986; Ghan et al., 1993; Boucher and Lohmann, 1995; Nenes et al., 2001; Ramanathan et al., 2001; Sullivan et al., 2016), this is different from CCN due to the limitation of the water vapor

in the actual environment. Using the prescribed supersaturation to calculate CDNC may therefore provide a bias on evaluation the aerosol indirect effect. For example, Kalkavouras et al. (2017, 2019) reported an average 12% enhancement of CDNC during two consecutive NPF episodes in the eastern Mediterranean, which was significantly smaller than the enhancement of  $N_{CCN}$  (~87%) during the NPF events. Hence, it is critical to fully consider the background meteorological conditions (e.g. using dynamic water vapor under different updraft velocities) to simulate the  $S_{max}$  when evaluating the effect of NPF on clouds and the associated climate effects.

Relevant studies have been carried out in clean regions, but fewer in polluted urban areas. While field studies have shown that NPF events can occur frequently in polluted urban sites although the high concentration of background particles are not conducive to the generation of new particles (Wu et al., 2011; Peng et al., 2014; Zimmerman et al., 2020), and the formation and growth rate of new particles may be larger than that of relatively clean atmosphere. Wiedensohler et al. (2012) found that, under the high concentration levels of gaseous pollutants and strong oxidation in polluted area, the high concentration of nanoparticles generated by NPF events can rapidly grow to tens or even hundreds of nanometers in a few hours. Zhang et al. (2019) observed the subsequent growth of newly formed particles can last 2-3 days in urban Beijing, producing more CCN-sized particles. Previous studies in polluted regions demonstrated the complex and non-linear relationship between aerosol particles and CCN due to multiple emission sources (Zhang et al., 2014, 2016, 2017, 2019; Ren et al., 2018; Fan et al., 2020), highlighting the importance of understanding of the connections between aerosols and CCN or cloud droplet close to the source regions. Particularly, owing to the extremely high CN number concentrations (with order of magnitude as high as  $10^4$  or even  $10^5$   $\text{cm}^{-3}$ ) during NPF events in urban area, the effect of competition for water vapor and reduction in cloud supersaturation is expected to be more exacerbated.

The current study quantifies the contribution of NPF to  $N_{CCN}$  and CDNC in the polluted urban atmosphere of Beijing using field measurements of aerosol number size distributions and chemical composition. The effect of water vapor competition on evaluating  $N_d$  during NPF events is examined. The impact of the background pre-existing particles on the enhancement of CCN and CDNC is also discussed by contrasting the results on typical “clean” NPF day and “polluted” NPF day. Given the strong local primary sources like traffic emissions in urban area, a case study is conducted to investigate the impact of primary emissions on the evaluation of NPF effect on  $N_d$ .

## 2 Methodology

### 2.1 Site and experiment

A field campaign was conducted from May 25, 2017 to June 18, 2017 at the Institute of Atmospheric Physics (IAP),  
85 Chinese Academy of Sciences (39.98° N, 116.39° E) for measurements of aerosol physical and chemical properties. The  
IAP located between the north Third Ring Road and Fourth Ring Road in northern Beijing, which is a typical urban  
background site, mainly affected by traffic and cooking emissions. Beijing is hot in summer with high ambient relative  
humidity, which is conducive to generate atmospheric convection and reduce the high background aerosol condensation  
sink. The radiation in summer is stronger than other seasons, which promotes the generation of nucleated particles.  
90 Besides, local sources from traffic and cooking emissions, which may contribute many CCN size-relevant particles, can  
be important at the site (Sun et al., 2015). The instruments during the campaign were deployed in a container at ground  
level (~8 m on a meteorological tower).

The number size distribution of particles in the size range from 10 to 550 nm (scanned range) were measured with  
time resolution of 5 minutes by a scanning mobility particle sizer (SMPS; Wang and Flagan, 1990; Collins et al., 2002),  
95 which consists of a differential mobility analyzer (DMA, model 3081L, TSI Inc.) to classify particles with different sizes  
of particles, and a condensation particle counter (CPC, model 3772, TSI Inc.) to detect the size-classified particles. The  
sampled particles were dried to a relative humidity < 30% before entering the DMA. The non-refractory chemical  
composition of PM<sub>1</sub> is measured by an Aerosol Chemical Speciation Monitor (ACSM), which consists of an aerodynamic  
lens to efficiently sample and focus submicron particles into the ACSM (Ng et al. 2011). Before sampling into the ACSM,  
100 aerosol particles are dried by silica gel desiccant. The ACSM was operated at a time resolution of 15 min. And the  
non-refractory chemical components that can be measured mainly include organics, sulfate salts (SO<sub>4</sub><sup>2-</sup>), nitrate salts  
(NO<sub>3</sub><sup>-</sup>), ammonium (NH<sub>4</sub><sup>+</sup>), and chloride (Cl<sup>-</sup>) (Ng et al. 2011). The refractory components mainly include black carbon  
(BC), and the BC mass concentration was measured using a seven-wavelength aethalometer (AE33, Magee Scientific  
Corp).

### 105 2.2 Calculation of $N_{CCN}$

According to the hygroscopic growth process of particles described by Köhler theory (Köhler, 1936), the particles  
with the dry particle diameter ( $D_p$ ) larger than the critical dry particle diameter ( $D_c$ ) can be activated to form a cloud

droplet. In this study, the  $\kappa$ -Köhler theory (Petters and Kreidenweis, 2007), which simply describe the approximate relationship between the  $D_c$  with the critical supersaturation ( $S_c$ ), is applied as follows, when  $\kappa > 0.1$ :

110

$$K = \frac{4A^3}{27D_c^3 \ln^2 S_c}, A = \frac{4\sigma_w M_w}{RT\rho_w} \quad (1)$$

where  $M_w$  is the molecular weight of water ( $M_w = 0.018015 \text{ kg mol}^{-1}$ ),  $\rho_w$  is the density of water ( $\rho_w = 997.1 \text{ kg m}^{-3}$ ),  $T$  is the parcel temperature ( $T = 298.15 \text{ K}$ ), where  $\sigma_w$  is the droplet surface tension at the point of activation ( $\sigma_w = 0.072 \text{ J m}^{-2}$ ) and  $R$  is the universal gas constant ( $R = 8.315 \text{ J K}^{-1} \text{ mol}^{-1}$ ).  $\kappa$  is a hygroscopic parameter which depends on the chemical composition of the particle. In this study, based on the assumption that particles are internally mixed and their chemical composition will not be impacted by changes in particle size, we derived the  $\kappa$  with a simple mixing rule on the basis of chemical volume fractions (Petters and Kreidenweis, 2007; Gunthe et al., 2009). We used ACSM data, combined with the positive matrix factorization (PMF) analysis data to calculate the volume fraction of organic and inorganic, according to the following equation:

115

$$\kappa_{chem} = \sum_i \varepsilon_i \kappa_i \quad (2)$$

120

where  $\kappa_i$  and  $\varepsilon_i$  are the hygroscopic parameter and volume fraction for each individual (dry) component in the mixture, respectively. The  $\kappa$  value and density ( $\rho$ ) of each species used in the calculation are given in Table 1, which is referred from Petters and Kreidenweis (2007) and Topping (2005):

Table 1. Densities of different chemical species and their  $\kappa$  measured by the laboratory

125

Species	NH <sub>4</sub> NO <sub>3</sub>	(NH <sub>4</sub> ) <sub>2</sub> SO <sub>4</sub>	NH <sub>4</sub> HSO <sub>4</sub>	H <sub>2</sub> SO <sub>4</sub>	POA*	SOA*	BC
$\rho$ (kg m <sup>-3</sup> )	1720	1769	1780	1830	1000	1400	1700
$\kappa$	0.58	0.48	0.56	1.19	0	0.09	0

POA\* refers to primary organic aerosol and SOA\* refers to secondary organic aerosol

In the Eq. (1), the corresponding  $D_c$  can be obtained from a given  $S_c$ , and all particles with diameters larger than  $D_c$  can be activated. So the  $N_{CCN}$  can be calculated by integrating the PNSD from  $D_c$  to the largest particle size measured:

130

$$CCN(D_c) = \int_{D_c}^{550} n(\log D_p) d\log D_p \quad (3)$$

where  $n(\log D_p)$  is the particle number that correspond to each particle size bin  $d\log D_p$  in the aerosol number size distribution.

### 2.3 Calculation of $N_d$

The  $N_d$  depends on the  $S_{max}$  that can be formed in adiabatic ascending clouds. And this “cloud-relevant”

135 supersaturation varies at different updraft velocity. A global scheme of cloud droplet parameterization has been established and developed for the calculation of the  $N_d$  and  $S_{max}$  (Nenes and Seinfeld, 2001, 2003; Fountoukis and Nenes, 2005). In this study, the  $S_{max}$  was calculated from an equation that expresses the water vapor balance in adiabatic ascending cloud (Nenes and Seinfeld., 2003):

$$\frac{ds}{dt} = \alpha V - \gamma \frac{dw}{dt} \quad (4)$$

140 where  $\alpha$  and  $\gamma$  are two coefficients can be calculated by meteorological constants, the product of  $\alpha$  and  $V$  expresses the increase of supersaturation due to the adiabatic cooling of the parcel, while the  $\frac{dw}{dt}$  denotes the water condensation rate during the aerosol activation and subsequent growth processes. which is shown in detail in Eq (5). And the  $\frac{ds}{dt}$  express the growth rate of supersaturation, when it is equal to 0, the supersaturation reaches the maximum value.

$$\frac{dw}{dt} = \frac{\pi}{2} \rho_w \int_0^S D_p^2 \frac{dD_p}{dt} n^S(S') dS' \quad (5)$$

145 where  $\rho_w$  is the density of water.  $n^S(S')dS'$  is the number concentration of particles activated between  $S'$  and  $S' + dS$ .

Nenes et al. (2001) used a sectional representation of the CCN spectrum (i.e. particle number supersaturation distribution  $n^S(S')$ ) and total number of particles with  $S_c$  smaller than  $S$ ,  $F^S(S)$ , which is given by

$$F^S(S_x) = \int_0^{S_x} n^S(S') dS' \quad (6)$$

150 Where the  $S_x$  is the supersaturation in the environment, the  $n^S(S')$  in Eq. (6) represents the number concentration of particles activated between  $S'$  and  $S' + dS'$  in CCN spectrum. The  $F^S(S_x)$  can be calculated by the integration of  $n^S(S')$  from the lower limit 0 to upper limit  $S_x$ . If the  $S_{max}$  is known, the activated  $N_d$  can be calculated from Eq. (7), as

$$N_d = F^S(S_{max}) \quad (7)$$

155 In this study, we used the PNSD, chemical components, and empirical values of cloud updraft velocity to determine the  $S_{max}$  and  $N_d$  during NPF days in urban Beijing. Owing to that the direct measurement of cloud-scale updraft velocity in the atmosphere is almost impossible, the prescribed updraft velocity used in this study is referred from previous studies. Generally, the updraft velocities are reported very small (Martin et al., 1994) and range from 0.1 to 1.0 m s<sup>-1</sup> in stratocumulus and cumulus clouds in remote or marine boundary layer (Meskhidze et al., 2005; Morales et al., 2010). The vertical updraft velocities were derived varying from 0.3 to 3 m s<sup>-1</sup> (Zheng et al., 2015), which are typical for  
160 cumulus and convective clouds in summer of north China and thus was selected and applied in this study.

## 2.4 Method for calculating the contribution of NPF to $N_{CCN}$ and $N_d$

The increment of  $N_{CCN}$  or  $N_d$  by the NPF ( $\Delta N_{CCN}$  or  $\Delta N_d$ ) is usually quantified by comparing the  $N_{CCN}$  or  $N_d$  prior and after the NPF event (Peng et al., 2014; Wu et al., 2015; Ma et al., 2016; Ren et al., 2018; Zhang et al., 2019; Fan et al., 2020). In this study, the  $N_{CCN}$  or  $N_d$  prior the NPF event was determined as two-hours average of  $N_{CCN}$  or  $N_d$  before the burst of newly formed nucleated particles. And the  $N_{CCN}$  and  $N_d$  after the NPF event was calculated as the average of  $N_{CCN}$  or  $N_d$  from begin to the end of the NPF impact the  $N_{CCN}$  or  $N_d$ . So it is critical to determine when a NPF event start and end, or when a NPF begins and ends the impact on the  $N_{CCN}$  or  $N_d$ .

Generally, the burst in the nucleation mode particles symbolizes the beginning of an NPF event. Here, the moment when a half-hour concentration of the nucleation-mode particles suddenly increases with order of magnitude as high as  $\sim 10^4 \text{ cm}^{-3}$  during NPF cases was defined as  $t_{start}$ . The end time of an NPF event,  $t_{end}$ , is defined by the moment when the half-hour concentrations of nucleated particle is lower than that at  $t_{start}$ .

Since there need some time for the newly formed nucleated particles to grow to sufficient size to act as CCN, the  $N_{CCN}$  would not be enhanced as soon as new particles are generated. To determine the time that NPF begins and end the impact on the  $N_{CCN}$ , denoted as  $t_{start,CCN}$  and  $t_{end,CCN}$  respectively, the time series of  $N_{CCN}$  was firstly divided by the  $N_{CCN}$  at  $t_{start}$  at each prescribed supersaturation, to derive the normalized time series of  $N_{CCN}$ , denoted as  $R_S$ . The equation is written as follows,

$$R_S = \frac{CCN_S}{CCN_{S,t_{start}}} \quad (8)$$

where  $S$  represents the supersaturation. Before the new particles reaches a large enough size to impact  $N_{CCN}$ , the variations of  $R_S$  should remain constant for different supersaturations if the concentrations of the background or pre-exist aerosols changes insignificant. And at  $t_{start,CCN}$  when NPF begin to impact the  $N_{CCN}$ , an apparent increase in  $R_S$  is observed by taking the observation on June 11 as an example (Fig. 1a). Also, due to the heterogenous composition and distinct CCN activity of the newly formed particles (Duan et al., 2018; Ren et al., 2018; Zhang et al., 2019; Tao et al., 2021), a parameter,  $R_D$ , which was calculated with the relative standard deviation of the  $R_S$  of different supersaturations at a given time, is applied to fix the  $t_{start,CCN}$  and  $t_{end,CCN}$ . Then the  $t_{start,CCN}$  and  $t_{end,CCN}$  correspond to the moments when the  $R_D$  starts to increase and back to nearly zero (Fig. 1b) respectively between the  $t_{start}$  and  $t_{end}$ . The same method is used to determine the time that NPF begins and ends the impact on the  $N_d$ , which are denoted as  $t_{start,N_d}$  and  $t_{end,N_d}$  respectively (Fig. 1d, e). More details about the method can be found in Kalkavouras et al. (2019). As shown in Fig. 1, it is clearly that both the  $N_{CCN}$  and  $N_d$  exhibits large increase in the NPF-impacted time zone between  $t_{start,CCN}$  and  $t_{end,CCN}$  (Fig. 1c), and between  $t_{start,N_d}$  and  $t_{end,N_d}$  (Fig. 1f). The average time lag between  $t_{start}$  and  $t_{start,N_d}$  was about 3-5

190 hours which is shortened by 50% compared to that reported by Kalkavouras et al. (2019). This case on 11 June was not an individual case, and similar patterns are also shown on other NPF days during the campaign (Fig. S3-S8).

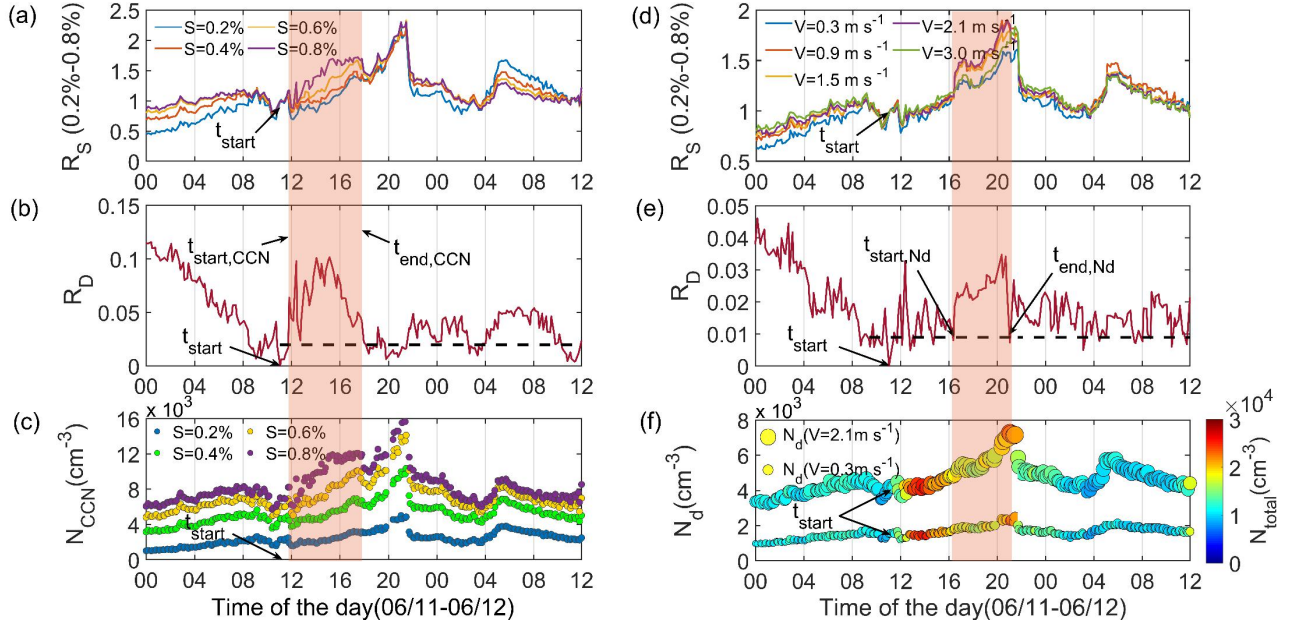


**Figure 1.** The diurnal evolution of (a) the  $R_S$  of  $N_{CCN}$  at different supersaturations, (b) the relative dispersion of  $R_S$ ,  $R_D$ , for  $N_{CCN}$  at different supersaturations, (c) the calculated  $N_{CCN}$  under different supersaturations, (d) the  $R_S$  of  $N_d$  under updraft velocities from 0.3 to 3.0  $\text{m s}^{-1}$ , (e) the  $R_D$  for  $N_d$ , and (f) the calculated  $N_d$  at updraft velocities of 0.3 and 2.1  $\text{m s}^{-1}$  on 11 June, 2017.

Note that this method is with an assumption of the unchanged background pre-exist aerosols during the NPF events, without consideration of the impacts from local emission sources, and diurnal changes in the planetary boundary layer (PBL). As shown in Fig. 2b, the time series of  $N_{CN}$  presents a baseline which indicates that concentrations of the background aerosols on each of the 7 typical NPF day don't vary much, the impact from the variation of background aerosol particles thus should be insignificant. The impact of PBL is expected to be small when the growth of the newly formed particles spans only a few hours. However, when the growth continues longer time to evening or at night which may coincide with the period that the PBL height changes from high to low (Kerminen et al., 2012; Altstädter, et al., 2015; Li et al., 2017), it will result in a larger  $N_{CCN}$  and  $N_d$ , leading to an overestimation of the contribution of NPF to  $N_{CCN}$  and  $N_d$ . A quantitative evaluation of such impact is difficult due to that the contemporary PBL data is not available. Therefore, here we only investigate the impact of local emissions on the evaluation of NPF effect on  $N_d$  based on a case study.



### 3 Results and discussion

#### 3.1 Time series of observed NPF events and calculated $N_{CCN}$ and $N_d$

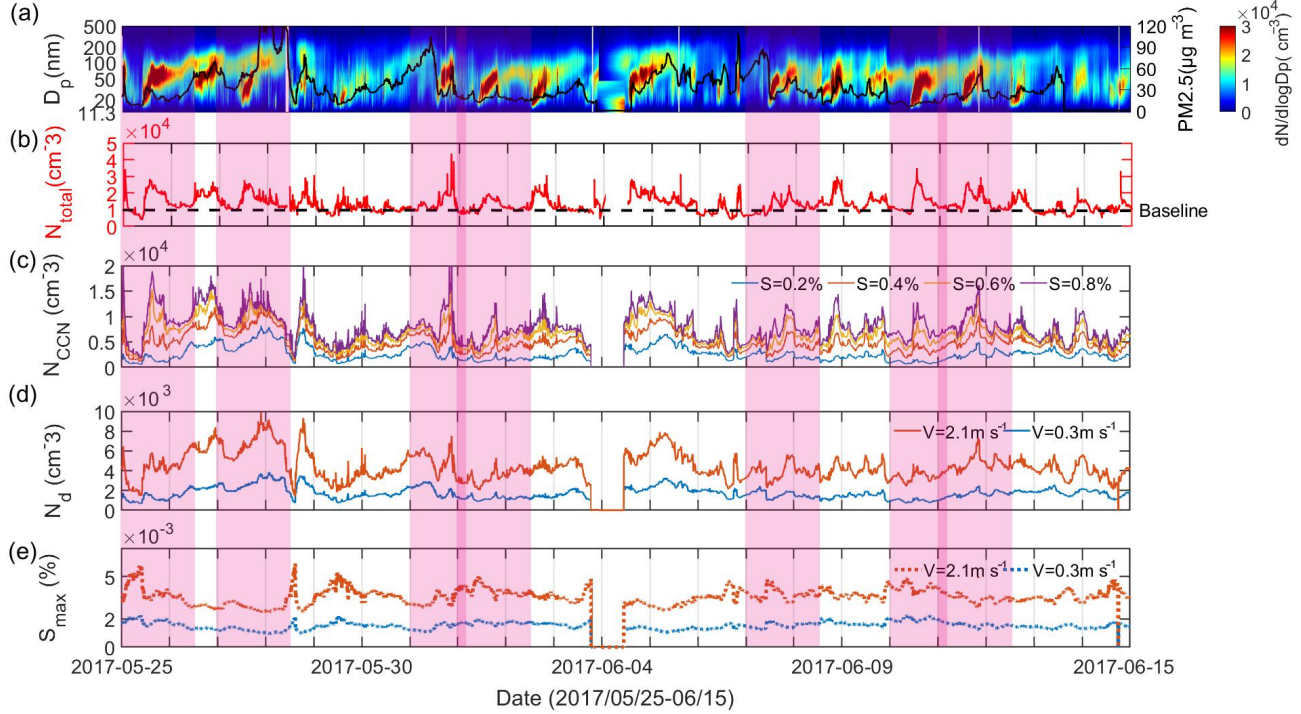


**Figure 2.** Time series of (a) particle number size distribution (PNSD) (the selected 7 typical NPF events are marked in pink shadow), (b) the total particle number concentration ( $N_{total}$ ), (c) CCN number concentration ( $N_{CCN}$ ), (d) cloud droplets number concentration ( $N_d$ ) and (e) the maximum supersaturation ( $S_{max}$ ) from 25 May to 15 June 2017.

During the observed periods from 25 May to 15 June 2017, the NPF events occurred on most of days (~13 days) (Fig. 2a). According to Dal et al. (2005) and Wu et al. (2015), a typical NPF event includes the sudden appearance and continuous growth of particles smaller than 25 nm, and a “banana” shape can be seen on the particle number size spectrum. While non-NPF events may also have sudden increases of fine particles at a short time scale (e.g. local sources from vehicle or cooking emissions), but they do not show the “banana” shape. Therefore, those cases with typical “banana” shape (7 NPF events in total), which presents a complete NPF evolution process from nucleation to subsequent growth (not interrupted by meteorological conditions either), are selected for further study (marked in pink shadow in Fig. 2). Fig. 2b, c and d present the time series of  $N_{CN}$ ,  $N_{CCN}$  and  $N_d$ . It exhibits that the NPF event drives the variation of  $N_{CCN}$  and  $N_d$ , showing that the occurrence of NPF events as an important source of CCN. The variation trend of  $N_{CN}$  is more correlated with that of  $N_{CCN}$  than  $N_d$  (also see Fig. 4, Table S5). This is because that the  $N_{CCN}$  was calculated based on a constant  $S$  rather than refer to the availability of water vapor, while the calculation of  $N_d$  is based on the  $S_{max}$  that can

225 reach in the real atmosphere at a given updraft velocity. In the cloud, the change in the quantity of cloud particles can be directly reflected by the change in  $S_{max}$ . As shown in Fig. 2e, the average  $S_{max}$  for the two vertical updraft velocity of  $V=0.3 \text{ m s}^{-1}$  and  $V=2.1 \text{ m s}^{-1}$  was calculated to be under 0.2% and 0.4%, varying largely with the variation of  $N_{CCN}$  due to the effect of water vapor competition, which will be discussed in Section 3.3.

### 3.2 Quantitative evaluation of the NPF impact on $N_{CCN}$ and $N_d$

230 Based on the method in Section 2.4, the contribution of the NPF to  $N_{CCN}$  and  $N_d$  is calculated and shown in Fig. 3. The results show that the  $N_{CCN}$  is averagely increased by 32.0%, 43.0%, 53.0%, and 65.0% at S of 0.2%, 0.4%, 0.6% and 0.8% respectively during NPF events (Fig. 3b, c, Table S3), amounting to about 24%-37% of environment CCN at the cloud-relevant supersaturations are directly originated from NPF during the studied period in urban Beijing. And the rest (about 63-76%) of CCN are from the other sources or pre-existing particles, which is much larger than that derived in  
 235 remote Finokalia, Crete, Greece by Kalkavouras et al (2019). In other words, due to the higher background concentration of aerosol particles in polluted urban area, the relative contribution of NPF to  $N_{CCN}$  is more significant in remote clean regions.

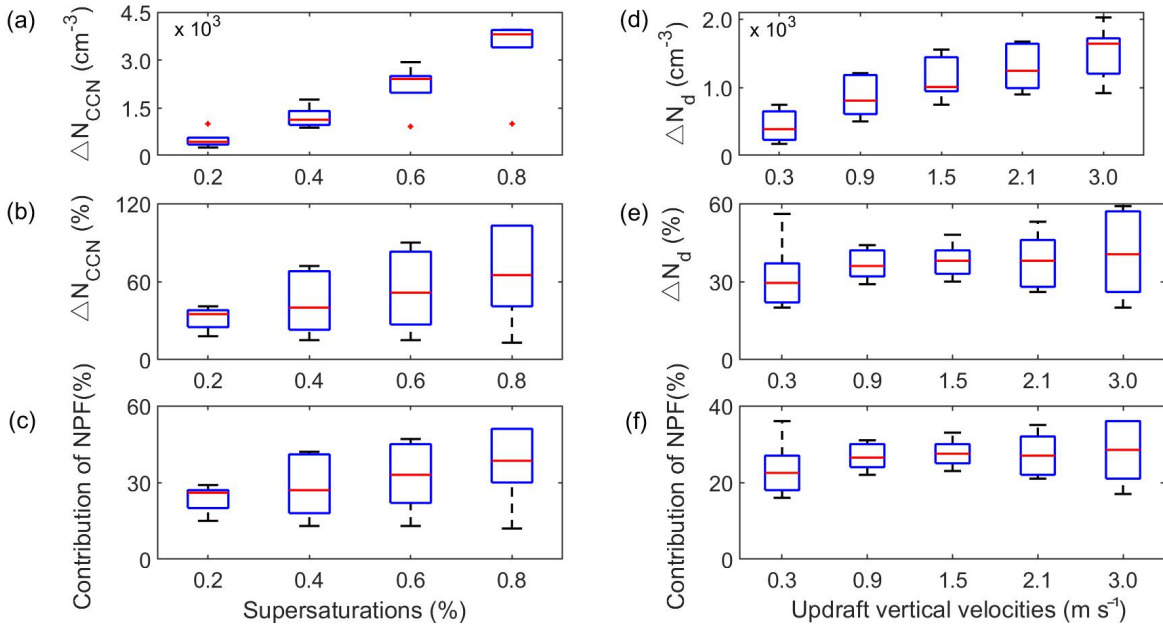


**Figure 3.** Box diagram of the increment of (a) CCN number concentration  $N_{CCN}$  ( $\Delta N_{CCN}$ ), (b) enhanced percentage of  $N_{CCN}$  and (c) the contribution to total  $N_{CCN}$  by NPF for different supersaturations (0.2%-0.8%), and (d) cloud droplet number concentration  $N_d$  ( $\Delta N_d$ ), (e) enhanced percentage of  $N_d$  and (f) the contribution to total  $N_d$  by NPF under different updraft velocities ( $0.3 \text{ m s}^{-1}$ - $3.0 \text{ m s}^{-1}$ ).

The estimated results of  $N_d$  for selected vertical updraft velocity are shown in Fig. 3d-f. Generally, the average  $S_{max}$

was calculated to be under 0.4% and 0.2% for  $V=2.1 \text{ m s}^{-1}$  and  $V=0.3 \text{ m s}^{-1}$  respectively (Fig. 2e), corresponding to  
245 critical particle sizes ( $d_c$ ) of  $\sim 70 \text{ nm}$  and  $\sim 110 \text{ nm}$ . It means that most activated drops are from accumulation-mode  
particles and larger particles in Aitken-mode. The large contribution of the Aitken-mode particles leads to large amount of  
cloud droplets in urban Beijing, especially for high updraft velocity. Basically, the averaged  $\Delta N_d$  (increased by NPF) are  
433, 854, 1117, 1281, and  $1523 \text{ cm}^{-3}$  at updraft velocities of 0.3, 0.9, 1.5, 2.1, and  $3 \text{ m s}^{-1}$  respectively (Fig. 3d), which is  
a much larger magnitude compared with that in the clean areas (Morales et al., 2014; Sullivan et al., 2016; Kalkavouras et  
250 al., 2019). This is equal to that the  $N_d$  are enhanced by 32%, 37%, 38%, 38%, 40% at updraft velocities of 0.3, 0.9, 1.5,  
2.1, and  $3 \text{ m s}^{-1}$  respectively (Fig. 3e), suggesting that the higher cloud updraft velocity not only generates more cloud  
droplets, but also induces larger enhancements in  $N_d$ . We also show that the NPF contributes about 30% to the total  $N_d$   
during the studied period in urban Beijing (Fig. 3f). And the rest (about 70%) of cloud droplet are from the other sources  
or pre-existing particles. With the increase of the  $S$ , the percentages of NPF-initiated  $N_{CCN}$  and the contributions of the  
255 NPF to  $N_{CCN}$  increased more significantly than that for  $N_d$  with the increase of  $V$ . In other words, the percentages of  
NPF-initiated  $N_d$  and the contributions of the NPF to  $N_d$  are relatively independent on the variation of  $V$ . This is primarily  
due to the water vapor competition effect under very high CN number concentrations when calculating the  $N_d$ . Under  
high  $N_{CN}$ , the water vapor competition effect will lead to lower  $S_{max}$ , which is smaller than that the constant  $S$  for  
calculating  $N_{CCN}$ . Roughly, the  $N_d$  at  $V$  of  $0.3\text{-}3 \text{ m s}^{-1}$  corresponds to the  $N_{CCN}$  at  $S$  of 0.1%-0.5%, within which the  
260 percentages of  $\Delta N_{CCN}$  and the contributions of the NPF to  $N_{CCN}$  don't change much either. The effect of water vapor  
competition will be further examined in the following section.

### 3.3 The effect of water vapor competition on evaluating $N_d$

Fig. 4 shows the scatter plots of correlations between  $N_{CN}$  and  $N_{CCN}$  at supersaturations of 0.6% and 0.8% and the  
correlations between  $N_{CN}$  and  $N_d$  under updraft vertical velocities of  $2.1 \text{ m s}^{-1}$  and  $3.0 \text{ m s}^{-1}$ . The  $N_{CCN}$  and  $N_{CN}$  were  
265 obviously linearly related, but the correlation between  $N_d$  and  $N_{CN}$  was non-linear. When shown as the average values  
with error bars, the  $N_d$  increase linearly as  $N_{CN}$  increase when the  $N_{CN}$  is below 15000, then the  $N_d$  began to decrease with  
the further increase of  $N_{CN}$ . This has been presented in previous studies (Nenes et al., 2001; Ramanathan et al., 2001;  
Sullivan et al., 2016), and was believed to be caused by the water vapor competition of the aerosol particles. Although the  
larger updraft velocities can achieve greater supersaturation in adiabatic ascending clouds and more particles can be  
270 activated into cloud droplets, the water vapor competition still occurred when background aerosol particles increased to a  
certain number. This is fully suggested by the difference between the calculated  $N_{CCN}$  using the constant  $S$  and the  $N_d$

using the variable  $S_{max}$  in the air parcels. Because in the actual environment, it is often unable to achieve the sufficient supersaturation compared to the prescribed ones that are preset in the instrument. For example, the average  $S_{max}$  is lower than 0.5% at the maximum cloud updraft velocity of  $3 \text{ m s}^{-1}$  according to the calculation results in this study. Therefore, although NPF events may strongly increase  $N_{CCN}$ , the formed  $N_d$  are eventually limited by water vapor competition which determines the  $S_{max}$  that varies in the cloud. The  $S_{max}$  is related to the cloud formation dynamics and the aerosol levels in the region.

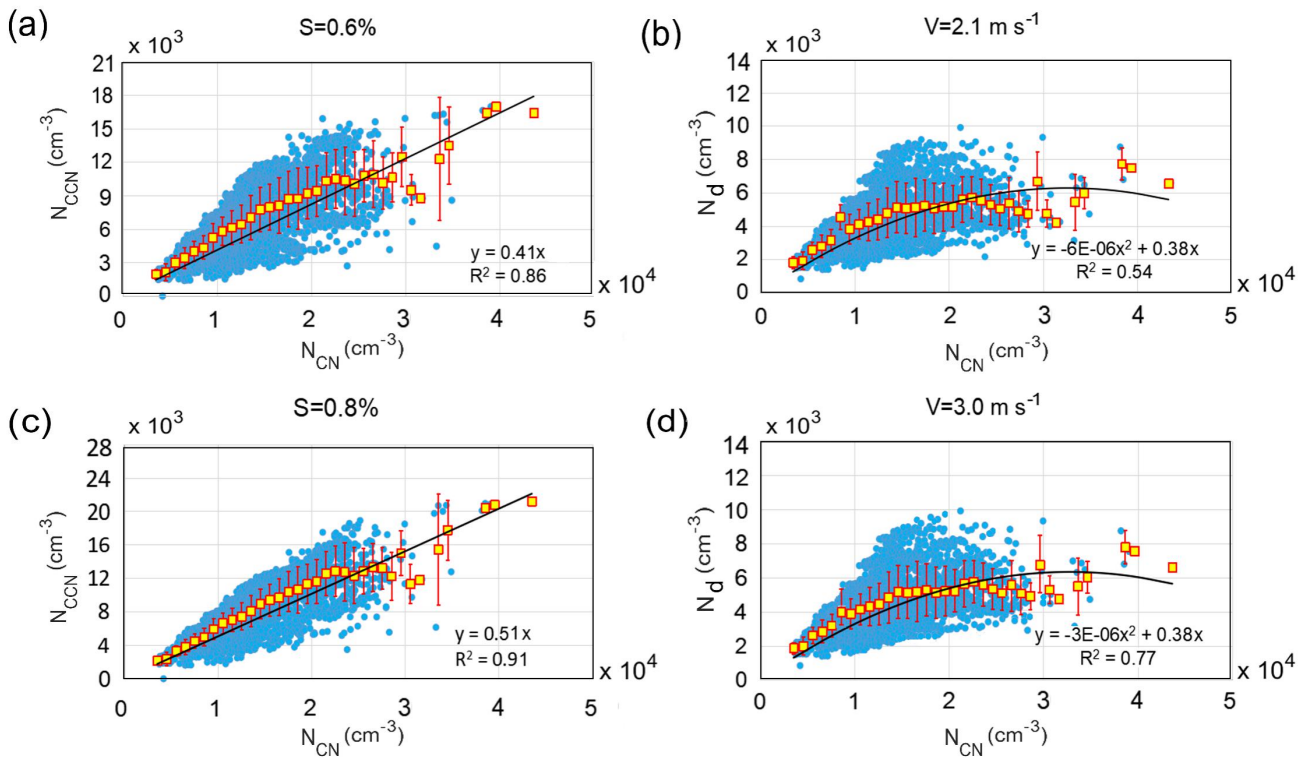


**Figure 4.** Scatter plots of correlation between total number concentration ( $N_{CN}$ ) and CCN number concentration ( $N_{CCN}$ ) at supersaturation of (a) 0.6% and (c) 0.8% respectively. Scatter plot of correlation between  $N_{CN}$  and cloud droplet number concentration ( $N_d$ ) at updraft vertical velocity of (b)  $2.1 \text{ m s}^{-1}$  and (d)  $3.0 \text{ m s}^{-1}$  respectively.

To evaluate the effect of water vapor competition on  $N_d$ , by taking the case on 11 June as an example, we compare the  $N_d$  calculated from the varied  $S_{max}$  at different updraft velocities with the  $N_d$  at referred constant  $S$  (Fig. 5). The results from other NPF cases were also summarized in Table S6 and Table S7. Obviously, after the  $t_{start}$ , the  $S_{max}$  starts to decrease and was negatively correlated with  $N_d$  for both the updraft velocities, reflecting the enhanced effect of competition for water vapor from the growing number of droplets (Fig. 5a and 5b). It is shown that  $S_{max}$  was decreased by  $14.5 \pm 3.5\%$ ,  $13.3 \pm 4.0\%$ ,  $13.4 \pm 4.2\%$ ,  $12.0 \pm 4.1\%$ ,  $11.7 \pm 3.9\%$  for  $V=0.3, 0.9, 1.5, 2.1$  and  $3 \text{ m s}^{-1}$  respectively (Fig. 5c, d).

Therefore, by compared to the  $N_d$  calculated from the constant  $S$ , the  $N_d$  calculated from the variable  $S_{max}$  is greatly  
 290 reduced at both the updraft velocities of  $0.3 \text{ m s}^{-1}$  and  $2.1 \text{ m s}^{-1}$ , suggesting a significant suppression of cloud droplet  
 formation. Quantitatively, the  $N_d$  are reduced by  $19.0 \pm 4.5\%$ ,  $15.7 \pm 4.7\%$ ,  $14.8 \pm 5.6\%$ ,  $12.3 \pm 4.9\%$ ,  $11.8 \pm 5.0\%$  at updraft  
 velocity of  $0.3$ ,  $0.9$ ,  $1.5$ ,  $2.1$  and  $3 \text{ m s}^{-1}$  respectively on the NPF days. Our results are similar with that reported by  
 Kalkavouras et al. (2017), which shows this competition effects suppress  $N_d$  by 20% for  $V = 0.3 \text{ m s}^{-1}$  and 12.3% for  $V =$   
 0.6  $\text{m s}^{-1}$ . In addition, the declined percentages with increase of the updraft velocity suggests that the effect becomes  
 295 smaller at larger  $V$  that can achieve greater  $S_{max}$  in the environment. Essentially, water vapor competition led to the  
 reduction in  $N_d$  by decreasing the required  $S_{max}$  for the CN activation.

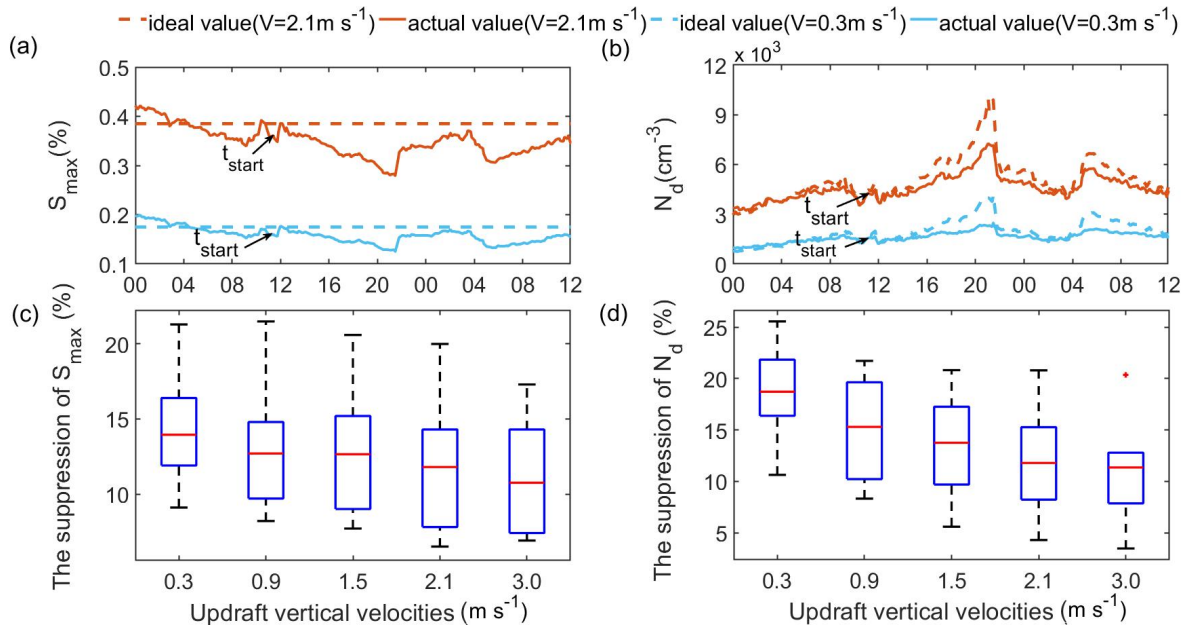


**Figure 5.** (a) The diurnal changes of the calculated maximum supersaturation ( $S_{max}$ ) (referred to the constant  
 supersaturation  $S$ ) at  $V=0.3 \text{ m s}^{-1}$  and  $2.1 \text{ m s}^{-1}$  on 11 June 2017; (b) Comparison of the cloud droplets number  
 300 concentration ( $N_d$ ) under the constant  $S$  and  $S_{max}$  on 11 June 2017; The suppression percentage of (c)  $S_{max}$  and (d)  $N_d$  due  
 to the competition of water vapor.

### 3.4 The variations of CCN and cloud droplet on typical “clean” and “polluted” NPF day: a case study

Generally, the lower  $\text{PM}_{2.5}$  means low background condensation sink (CS) which is conducive for the condensation  
 and coagulation of nucleation particles (Wu et al., 2011; Yue et al., 2011; Wiedensohler et al., 2012). Different from the  
 305 remote clean area, some of the NPF events in urban Beijing during the campaign occurred with background pollutions  
 (with daily mass concentrations of  $\text{PM}_{2.5}$  of  $\sim 40 \mu\text{g m}^{-3}$ ) or are impacted by local primary emissions. This kind of NPF  
 event has different characteristics from that in clean conditions, as the sudden increase of nucleation particles less than 25

nm is often accompanied by an increase of large particles at the beginning of NPF. Here, they are named as “polluted” and “clean” NPF event respectively. Two days, on 27 May and 11 June, representing the typical “polluted” and “clean” NPF events respectively, are selected for contrasting the effect of the two kinds of NPF on CCN and CDNC. As shown in Fig. 7, there is a higher pre-existing background of accumulation mode particles across the day on “polluted” NPF day of 27 May than that on “clean” NPF day of 11 June. On “clean” NPF day, much more nucleation and Aitken mode particles, with  $N_{CN}$  enhancement of 2-fold higher than that on “polluted” day (Fig. 7a), were generated and NPF events developed stronger in the initial stage. The beginning of NPF events ( $t_{start}$ ) on polluted case (11:00 a.m.) was about 2 hours later than that on clean case (~9:00 a.m.).

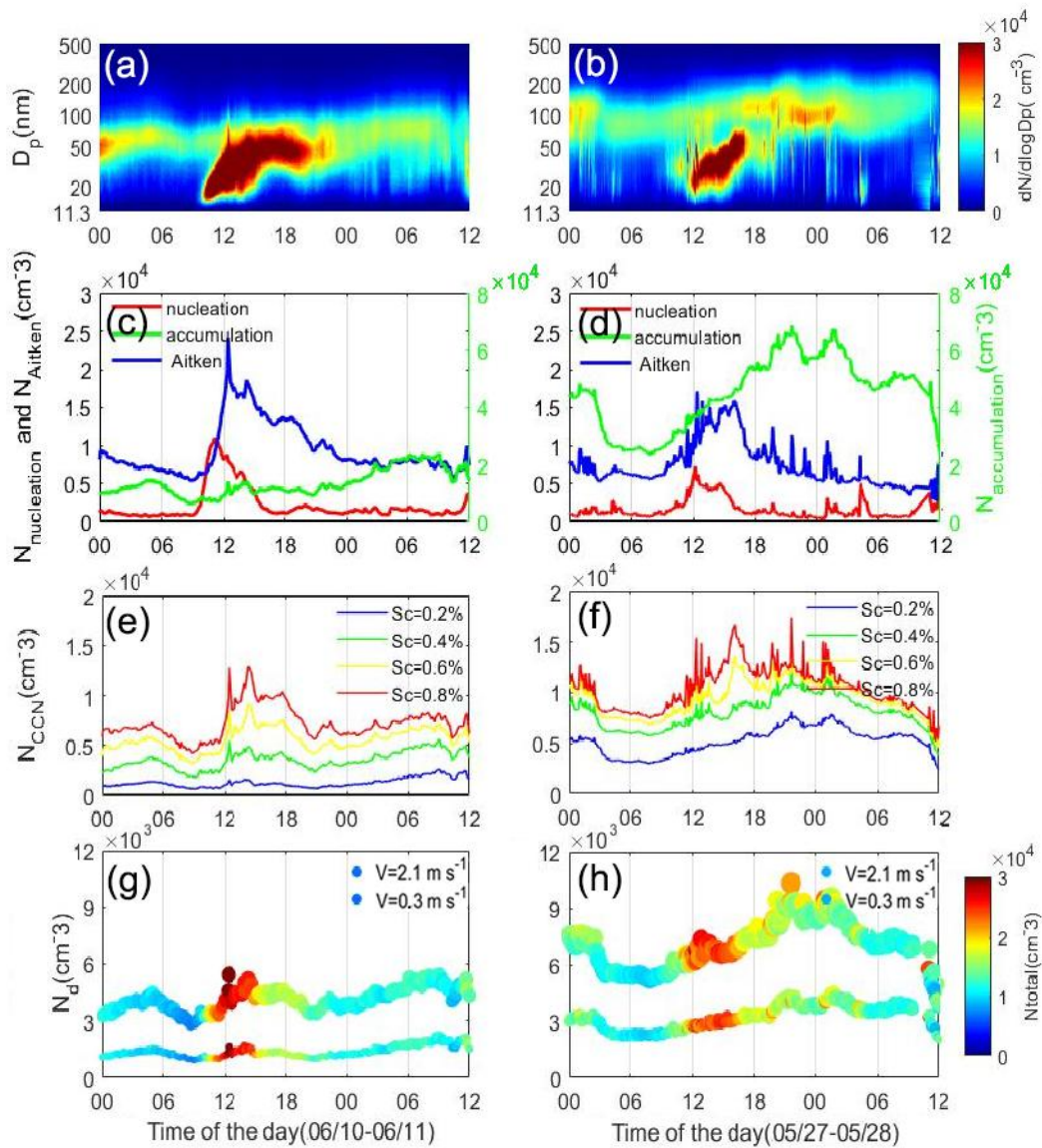


**Figure 6.** Comparison of (a, b) the particle number size distribution PNSD, (c, d) aerosol particle number concentration  $N_{CN}$ , (e, f) CCN number concentration  $N_{CCN}$  and (g, h) cloud droplet number concentration  $N_d$  between a clean and a

320 polluted NPF event. The “clean” NPF day is with a clean background ( $PM_{2.5}=14 \text{ } (\mu\text{g}/\text{m}^3)$ ), and the “polluted” NPF day is with  $PM_{2.5}$  of  $73 \text{ } (\mu\text{g}/\text{m}^3)$ .

For the both cases, the  $N_{CCN}$  are increased with the evolution of the NPF events (Fig. 6a, b, e, f). But the magnitude of the enhancements at the two cases are quite different. The  $N_{CCN}$  during NPF events under polluted day was generally twice than that of clean day (Fig. 6e and 6f), because there were a large number of pre-existing CCN-size aerosol particles on polluted NPF days. As a result, a larger increment of  $N_{CCN}$  is derived on clean NPF day, showing 37-80% and 15-41% increases percentage of  $N_{CCN}$  from NPF on clean and polluted days respectively (Fig. 7b). As for  $N_d$ , on clean days are 22% and 37%, and 34% and 26% on polluted days under updraft velocity of  $0.3$  and  $2.1 \text{ m s}^{-1}$ . The increase percentages in  $N_d$  between clean and polluted days are comparable. The result just further illustrates that the effect of water vapor competition on  $N_d$  under high  $N_{CN}$  in polluted atmosphere. This suggests that it is critical to fully consider the background meteorological conditions (e.g. using dynamic water vapor under different updraft velocities) to simulate the  $N_d$  when evaluating the effect of NPF on clouds and the associated climate effects.

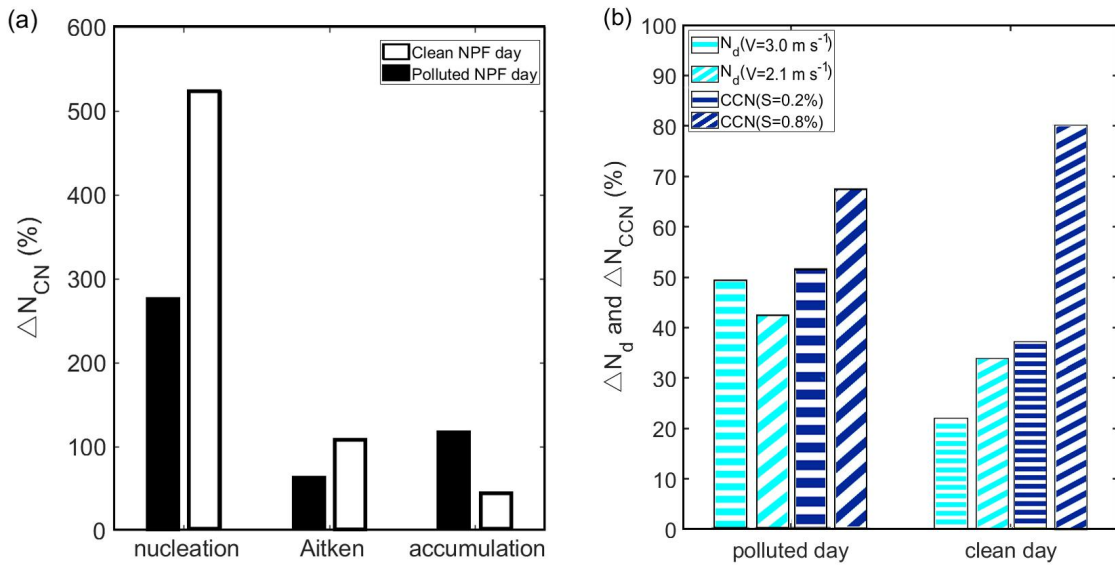


**Figure 7.** Comparison of the increments of (a) total particle number concentration ( $N_{CN}$ ), and (b) CCN number concentration ( $N_{CCN}$ ) and cloud droplet number concentration ( $N_d$ ) between the two different typical NPF events.

### 3.5 The impact of primary emissions during evening rush hour on the calculation of NPF contribution to $N_{CCN}$ and

335  $N_d$ : a case study

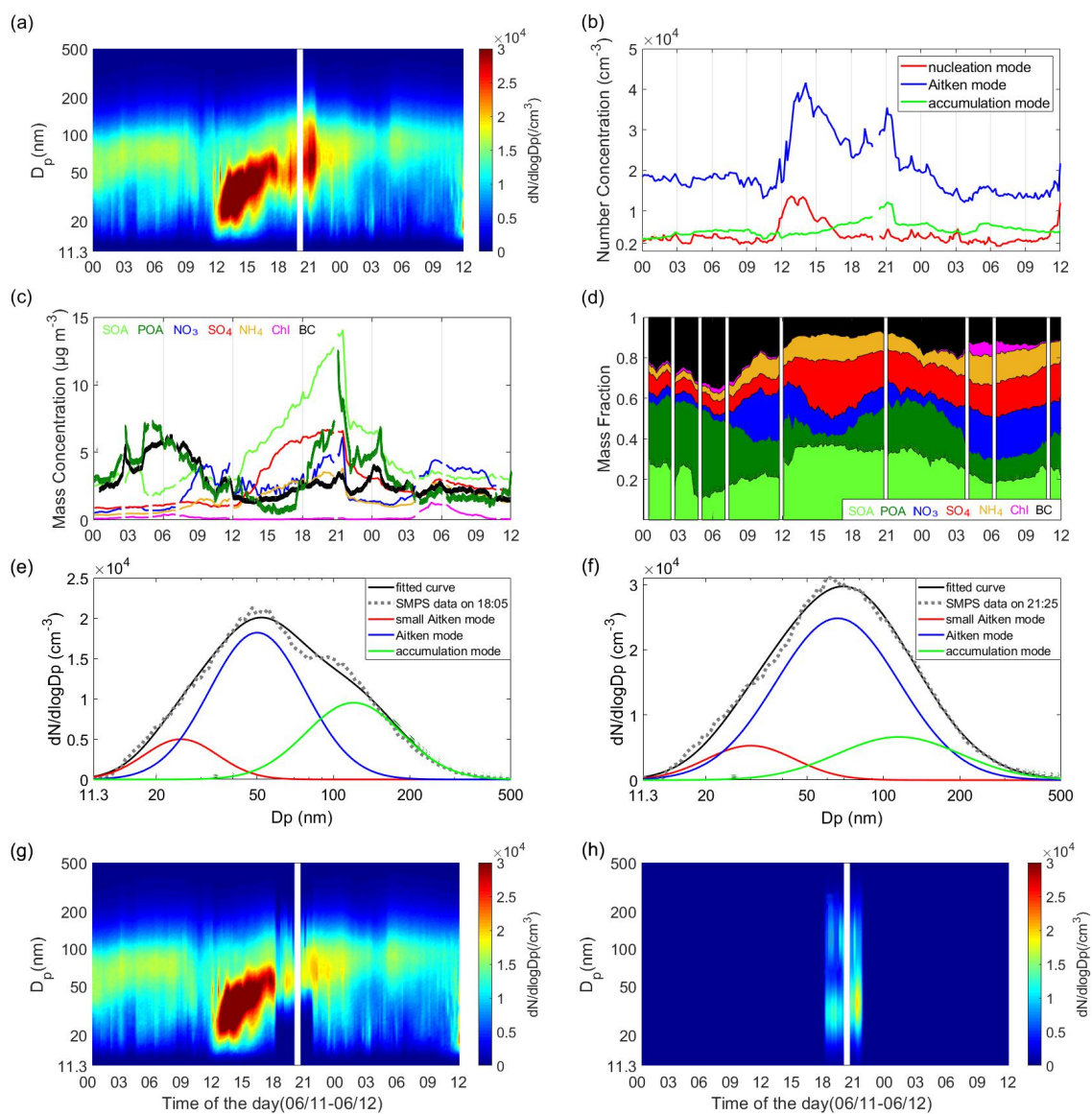
During the campaign, very high number concentrations of fine particles were observed during evening rush hour (as shown in Fig. 2a) when primary emissions related to automobile exhaust or cooking activities near the site may impact

the PNSD. Those particles from primary emissions can serve as CCN and thereby impact the evaluation of NPF contribution to  $N_d$ . Therefore, taking the day of June 11 as an example, such effect from primary emissions during evening rush hour is investigated (Fig. 8). On the day, one hour after the burst of newly formed particles at ~12:00 a.m., the  $N_d$  began to rise rapidly, and the increase of  $N_d$  continued until to 21:30 at night (Fig. 1f). At ~18:00, the primary emissions also begin to impact the  $N_{CCN}$  and  $N_d$ . Note that a sudden decrease and dilution in the PNSD is due to a precipitation event at ~21:30. From 18:00-21:30, the CCN and cloud droplets were from both NPF source and the primary emissions. The impact of primary emissions is also indicated by the variations of particles composition during 18:00-22:00, when both the primary organic aerosols (POA) and BC show a rapid increase in the mass concentration and fraction (Fig. 8c and 8d). Here, a positive matrix factorization (PMF) analysis was performed to separate the primary and secondary organic aerosol factors quantitatively for the purpose of source apportionment based on field measurement by an Aerodyne high-resolution time-of-flight aerosol mass spectrometer (HR-ToF-AMS) (Xu et al., 2017; Zhang et al., 2011). The PMF algorithm in the robust mode (Paatero and Tapper, 1994) was applied to the high-resolution mass spectra to resolve distinct OA factors representing primary and secondary sources and processes. More details about operation of the HR-ToF-AMS and PMF analysis also can be found in support information of Liu et al (2021).

To evaluate the impact of the primary emissions, it is critical to separate the particle modes representing the primary aerosols from the observed PNSD. According to the observed characteristics of PNSD, the newly formed particles continue to grow and dominated by Aitken mode for several hours after the NPF occurred (Fig. 8a). The size mode of the newly formed particles during the rush hour is estimated by applying a growth rate of  $3.2 \pm 0.5 \text{ nm h}^{-1}$ , which is calculated by the variation of median particle size during 12:00-18:00. The calculation results show that the NPF-tracked particles can grow to ~50-60 nm during the rush hour period. While, the primary particles from vehicles or cooking are generally with a smaller size (~30 nm) than the NPF-tracked particles mode and accumulation mode (~100-120 nm) (Brines et al., 2015; Dall'Osto, et al., 2011; Harrison, et al., 2011), so we applied three modes to fit the PNSD from the beginning of the evening rush hour to the end assuming a normal distribution. Note that the size mode for background aerosols almost coincides with the accumulation mode of primary emitted particles during the period. Since the mode and concentration of background aerosols do not change much before and after the occurrence of new particles (Fig. 8a, b), the impact of background aerosol is thus deducted from the fitting accumulation mode. The fitted result shows a major peak in the Aitken mode at ~50 nm that is related to the NPF event, and two minor peaks in Aitken (~30 nm) and accumulation (~100-120 nm) mode (Fig. 8e, f) that are associated with the primary vehicle or cooking emissions. Fig. 8g and Fig. 8h show the separated PNSD of the NPF-related and primary aerosols respectively. Then the increment of  $N_{CCN}$  and  $N_d$  from



NPF are obtained from the PNSD of NPF mode, and the increment of  $N_{CCN}$  and  $N_d$  from primary emissions are obtained by subtracting the increment of  $N_{CCN}$  and  $N_d$  by NPF from the total increment of  $N_d$ .



370 **Figure 8.** Diurnal variations of the (a) aerosol size distribution, (b) particle number concentrations for different size  
 modes, (c) mass concentrations of aerosol chemical composition, and (d) mass fraction of aerosol chemical components,  
 (e) (f) fitted three modes of the particle number concentration PNSD at 18:00 and 21:30, and (g) diurnal variations of the  
 separated NPF-related PNSD and (h) the PNSD of primary aerosols.

375

**Table 2.** Quantitative evaluation of the contribution of primary emissions to  $N_d$  and  $N_{CCN}$

$V$ or $S$	$D_c$	$\Delta N_{d\_NPF}$ or $\Delta N_{CCN\_NPF}$	$\Delta N_{d\_PE}^a$ or $\Delta N_{CCN\_PF}^a$	$\Delta N_{d\_total}$ or $\Delta N_{CCN\_total}$
------------	-------	--	--	--

$m\ s^{-1}, or\ \%$	$nm$	$cm^{-3}$ ,	$\%$	$cm^{-3}$ ,	$\%$	$cm^{-3}$
Evaluation of the contribution of primary emissions to $N_d$						
0.3	140	200	84.4%	37	15.6%	237
0.9	107	543	86.6%	84	13.4%	627
1.5	93	676	87.5%	97	12.5%	773
2.1	84	750	83.1%	153	16.9%	903
3.0	75	942	77.1%	279	22.9%	1221
Evaluation of the contribution of primary emissions to $N_{CCN}$						
0.2%	109	654	92.0%	57	8.0%	711
0.4%	69	1356	87.2%	199	12.8%	1555
0.6%	52	1680	87.1%	249	12.9%	1929
0.8%	43	1801	85.0%	318	15.0%	2119

<sup>a</sup>PE, primary emission

The calculated results are summarized in Table 2. For  $N_d$ , the average contribution of primary emission to  $N_d$  is 15.6%, 13.4%, 12.5%, 16.9% and 22.9%  $cm^{-3}$  for updraft velocities of 0.3, 0.9, 1.5, 2.1 and 3  $m\ s^{-1}$  respectively. The proportion of contribution from NPF and primary emission to  $N_d$  increment change with the variation of  $V$ . The higher proportion of contribution from primary emission is obtained at higher  $V$ , which may be determined by the different characteristics between atmospheric particles emitted from the evening traffic sources and generated from NPF events. For  $N_{CCN}$ , the average contribution from primary emissions is 8.0%, 12.8%, 12.9%, 15.0% at  $S$  of 0.2%, 0.4%, 0.6%, 0.8% respectively. Compared with  $N_d$ , the contribution percentage of primary emission to  $N_{CCN}$  is smaller due to that the total  $N_{CCN}$  is much more than the total  $N_d$ . Our result shows considerable impact of those primary sources when evaluating the NPF contribution to cloud droplet number, highlighting the importance of considering the influence from multiple (i.e. secondary and primary) sources on clouds in the polluted atmosphere. Finally, it is worth noting that the dynamic changes of PBL would also impact the  $N_{CCN}$  and  $N_d$  during the period, and the decrease in the height of PBL from the daytime to evening will result in an increase of  $N_{CCN}$  or  $N_d$ . However, for this case, the impact from primary emissions is much more prominent as indicated by the sharply raised particle number concentrations during the rush hour (Fig. 8b).

#### 4 Conclusions

In this study, we quantified the contribution of NPF to  $N_d$  at typical updraft velocities in clouds using field measurements of aerosol number size distributions and chemical composition in urban Beijing. We show that the NPF drives the variations of  $N_{CCN}$  and  $N_d$ . About 32%-65%  $N_{CCN}$  are increased by NPF events for supersaturation 0.2%-0.8% in polluted atmosphere. And the  $N_d$  is increased about 32%-40% by NPF at  $V= 0.3-3\ m\ s^{-1}$  accordingly. The significant

reduction in  $N_d$  is observed due to water vapor competition with consideration of actual environmental updraft velocity, with decrease rates of  $11.8\% \pm 5.0\%$  at  $V=3 \text{ m s}^{-1}$  and  $19.0\% \pm 4.5\%$  at  $V=0.3 \text{ m s}^{-1}$  by comparing with that from a constant supersaturation. The effect of water vapor competition becomes smaller at larger  $V$  at which the greater  $S_{max}$  can be achieved. Essentially, water vapor competition led to the reduction in  $N_d$  by decreasing the environmental  $S_{max}$  for the activation of aerosol particles. It is shown that  $S_{max}$  was decreased by  $14.5 \pm 3.5\%$  to  $11.7 \pm 3.9\%$  for  $V=0.3-3 \text{ m s}^{-1}$ . Our results suggest significant suppression of cloud droplet formation due to the water vapor competition particularly at extremely high aerosol particle number concentrations. As a result, although a larger enhancement of CCN-size particles by NPF event is derived on clean NPF day when there are few pre-existing background aerosol particles, no large discrepancy in the enhancement of  $N_d$  by NPF between the clean and polluted NPF day. Finally, we show a considerable impact of the primary sources when evaluating the NPF contribution to cloud droplet number from a case study. Our study highlights the importance of fully consideration of both the environmental meteorological conditions and multiple sources (i.e. secondary and primary) to evaluate the effect of NPF on clouds and the associated climate effects. For example, Merikanto et al. (2010) used model to simulate the variation of CDNC from the year of 1850 to 2000, and showed that NPF made a nearly equal contribution (16-13.5%) to global CDNC in all those years, leading to about 50% enhancement in the year from 1850 to 2000 change in cloud albedo. There are still large uncertainties about how to accurately quantitatively assess the response of these climate effects to NPF. This study is carried out in polluted urban area, which is a supplement to the research of the microphysical process of aerosol-cloud and provides a new perspective for the follow-up research in urban atmosphere. Note that, there are still limitations of our studies, as we only investigated several NPF cases within a short period due to the limited measurement data. The small sample size might cause bias in the results. Further studies based on more measurement data, i.e. with longer time periods and more observational sites, warrant to verify and refine our results, so as to parameterize the impact of NPF events on cloud, precipitation, and radiative forcing in models.

## Acknowledgments

This work was supported by the National Basic Research Program of China (2017YFC1501702), the National Natural Science Foundation of China (Grants 41675141, 41975174). All data used in the study are available on <https://data.mendeley.com/datasets/hkkzbn4zv3/1> or from the corresponding author upon request ([fang.zhang@bnu.edu.cn](mailto:fang.zhang@bnu.edu.cn)).

## Author statement

The authors declare no competing financial interest.

## 425 Author contribution

FZ and SJ conceived the conceptual development of the paper. LC, YS and JR contributed measurements. SJ directed and performed the experiments with LC, JL, JR, XY, ZL and FZ, SJ conducted the data analysis and wrote the draft of the paper. All authors commented on the paper.

## References

- 430 Albrecht, B. A.: Aerosols, cloud microphysics, and fractional cloudiness, *Science*, 245, 1227–1230, 1989.
- Altstädter, B., Platis, A., Wehner, B., Scholtz, A., Wildmann, N., Hermann, M., Käthner, R., Baars, H., Bange, J., and Lampert, A.: ALADINA – an unmanned research aircraft for observing vertical and horizontal distributions of ultrafine particles within the atmospheric boundary layer. *Atmos. Meas. Tech.*, 8, 1627–1639, <https://doi.org/10.5194/amt-8-1627-2015>, 2015.
- 435 Abdul-Razzak, H., Ghan, S., and Rivera-Carpio, C.: A parametrization of aerosol activation: 1. Single aerosol types, *J. Geophys. Res.*, 103, 6123–6131, 1998.
- Abdul-Razzak, H. and Ghan, S.: A parametrization of aerosol activation: 2. Multiple aerosol types, *J. Geophys. Res.*, 105, 6837–6844, 2000.
- Asmi, E., Kivekäs, N., Kerminen, V.-M., Komppula, M., Hyvärinen, A. P., Hatakka, J., Viisanen, Y., and Lihavainen, H.: 440 Secondary new particle formation in Northern Finland Pallas site between the years 2000 and 2010, *Atmos. Chem. Phys.*, 11, 12959–12972, <https://doi.org/10.5194/acp-11-12959-2011>, 2011.
- Boucher, O. and Lohmann, U.: The sulfate-CCN-cloud albedo effect, *Tellus*, 47B, 281–300, 1995.
- Bousiotis, D., Dall'Osto, M., Beddows, D. C. S., Pope, F. D., and Harrison, R. M.: Analysis of new particle formation (NPF) events at nearby rural, urban background and urban roadside sites, *Atmos. Chem. Phys.*, 19, 5679–5694, 445 <https://doi.org/10.5194/acp-19-5679-2019>, 2019.
- Brines, M., Dall'Osto, M., Beddows, D. C. S., Harrison, R. M., Gómez-Moreno, F., Núñez, L., Artíñano, B., Costabile, F., Gobbi, G. P., Salimi, F., Morawska, L., Sioutas, C., and Querol, X.: Traffic and nucleation events as main sources of ultrafine particles in high-insolation developed world cities, *Atmos. Chem. Phys.*, 15, 5929–5945,

- <https://doi.org/10.5194/acp-15-5929-2015>, 2015.
- 450 Cai, M., Liang, B., Sun, Q., Zhou, S., Chen, X., Yuan, B., Shao, M., Tan, H., and Zhao, J.: Effects of continental emissions on cloud condensation nuclei (CCN) activity in the northern South China Sea during summertime 2018, *Atmos. Chem. Phys.*, 20, 9153–9167, <https://doi.org/10.5194/acp-20-9153-2020>, 2020.
- Collins, D. R., Flagan, R. C., and Seinfeld, J. H.: Improved inversion of scanning DMA data, *Aerosol Sci. Tech.*, 36, 1–9, 2002.
- 455 Dal, M., Kulmala, M., Riipinen, I., Wagner, R., Hussein, T., Aalto, P. P., and Lehtinen, K. E. J.: Formation and growth of fresh atmospheric aerosols: eight years of aerosol size distribution data from SMEAR II, Hyytiälä, Finland, *Boreal Environ. Res.*, 10, 323–336, 2005.
- Dall'Osto, M., Thorpe, A., Beddows, D. C. S., Harrison, R. M., Barlow, J. F., Dunbar, T., Williams, P. I., and Coe, H.: Remarkable dynamics of nanoparticles in the urban atmosphere, *Atmos. Chem. Phys.*, 11, 6623–6637, 460 <https://doi.org/10.5194/acp-11-6623-2011>, 2011.
- Duan, J., Wang, Y., Xie, X., Li, M., Tao, J., Wu, Y., Cheng, T.: Influence of pollutants on activity of aerosol cloud condensation nuclei (CCN) during pollution and post-rain periods in Guangzhou, southern China, *Science of the Total Environment*, 642, 1008–1019, [10.1016/j.scitotenv.2018.06.053](https://doi.org/10.1016/j.scitotenv.2018.06.053), 2018.
- Fan, J., Leung, R., Rosenfeld, D., Chen, Q., Li, Z., Zhang, J., and Yan, H.: Microphysical effects determine 465 macrophysical response for aerosol impacts on deep convective clouds, *P. Natl. Acad. Sci. USA*, 110, E4581–E4590, <https://doi.org/10.1073/pnas.1316830110>, 2013.
- Fan, X., Liu, J., Zhang, F., Chen, L., Collins, D., Xu, W., Jin, X., Ren, J., Wang, Y., Wu, H., Li, S., Sun, Y., and Li, Z.: 470 Contrasting size-resolved hygroscopicity of fine particles derived by HTDMA and HR-ToF-AMS measurements between summer and winter in Beijing: the impacts of aerosol aging and local emissions, *Atmos. Chem. Phys.*, 20, 915–929, <https://doi.org/10.5194/acp-20-915-2020>, 2020.
- Fountoukis, C. and Nenes, A.: Continued development of a cloud droplet formation parameterization for global climate models, *J. Geophys. Res.*, 110, D11212, <https://doi.org/10.1029/2004JD005591>, 2005.
- Genz, C., Schrödner, R., Heinold, B., Henning, S., Baars, H., Spindler, G., and Tegen, I.: Estimation of cloud condensation nuclei number concentrations and comparison to in situ and lidar observations during the HOPE 475 experiments, *Atmos. Chem. Phys.*, 20, 8787–8806, <https://doi.org/10.5194/acp-20-8787-2020>, 2020.
- Ghan, S., Chung, C., and Penner, J.: A parameterization of cloud droplet nucleation part I: single aerosol type, *Atmos. Res.*, 30, 198–221, [https://doi.org/10.1016/0169-8095\(93\)90024-I](https://doi.org/10.1016/0169-8095(93)90024-I), 1993.

- Gunthe, S. S., King, S. M., Rose, D., Chen, Q., Roldin, P., Farmer, D. K., Jimenez, J. L., Artaxo, P., Andreae, M. O.,  
Martin, S. T., and Pöschl, U.: Cloud condensation nuclei in pristine tropical rainforest air of Amazonia: size-resolved  
480 measurements and modeling of atmospheric aerosol composition and CCN activity, *Atmos. Chem. Phys.*, 9,  
7551–7575, <https://doi.org/10.5194/acp-9-7551-2009>, 2009.
- Harrison, R. M., Beddows, D. and Dall'Osto, M.: PMF Analysis of Wide-Range Particle Size Spectra Collected on a  
Major Highway, *Environmental Science & Technology*, 45(14), 5522, [10.1021/es201998m](https://doi.org/10.1021/es201998m), 2011.
- Hudson, J. G. , Noble, S., and Tabor, S.: Cloud supersaturations from CCN spectra hoppel minima. *Journal of*  
485 *Geophysical Research Atmospheres*, 120(8), 3436–3452. <https://doi.org/10.1002/2014JD022669>, 2015.
- Kalkavouras, P., Bossioli, E., Bezantakos, S., Bougiatioti, A., Kalivitis, N., Stavroulas, I., Kouvarakis, G., Protonotariou,  
A. P., Dandou, A., Biskos, G., Mihalopoulos, N., Nenes, A., and Tombrou, M.: New particle formation in the southern  
Aegean Sea during the Etesians: importance for CCN production and cloud droplet number, *Atmos. Chem. Phys.*, 17,  
175–192, <https://doi.org/10.5194/acp-17-175-2017>, 2017.
- 490 Kalkavouras, P. , Bougiatioti, A. , Kalivitis, N. , Stavroulas, I. , and Mihalopoulos, N.: Regional new particle formation as  
modulators of cloud condensation nuclei and cloud droplet number in the eastern mediterranean. *Atmos. Chem. Phys.*,  
19(9), 6185-6203, <https://doi.org/10.5194/acp-19-6185-2019>, 2019.
- Kazil, J., Stier, P., Zhang, K., Quaas, J., Kinne, S., O'Donnell, D., Rast, S., Esch, M., Ferrachat, S., Lohmann, U., Feichter,  
J.: Aerosol nucleation and its role for clouds and Earth's radiative forcing in the aerosol-climate model  
495 ECHAM5-HAM, *Atmos. Chem. Phys.*, 10, 10733, <https://doi.org/10.5194/acp-10-10733-2010>, 2010.
- Kerminen, V. M., Paramonov, M., Anttila, T., Riipinen, I., Fountoukis, C., Korhonen, H., Asmi, E., Laakso, L.,  
Lihavainen, H., Swietlicki, E., Svenningsson, B., Asmi, A., Pandis, S. N., Kulmala, M., and Petäjä, T.: Cloud  
condensation nuclei production associated with atmospheric nucleation: a synthesis based on existing literature and  
new results, *Atmos. Chem. Phys.*, 12, 12037-12059, <https://doi.org/10.5194/acp-12-12037-2012>, 2012.
- 500 Kerminen, V. M., Chen, X., Vakkari, V., Petäjä, T., Kulmala, M., and Bianchi, F.: Atmospheric new particle formation and  
growth: review of field observations, *Environ. Res. Lett.*, 13, 103003, <https://doi.org/10.1088/1748-9326/aadf3c>, 2018.
- Khvorostyanov, V. I., and Curry, J. A.: A simple analytical model of aerosol properties with account for hygroscopic  
growth: 1. Equilibrium size spectra and cloud condensation nuclei activity spectra, *J. Geophys. Res.*, 104, 2175-2184,  
<https://doi.org/10.1029/98JD02687>, 1999.
- 505 Köhler, H.: The nucleus in and the growth of hygroscopic droplets, *Transactions of the Faraday Society*, 32: 1152-1161,  
<https://doi.org/10.1039/tf9363201152>, 1936.

- Kulmala, M. and Kerminen, V. M.: On the formation and growth of atmospheric nanoparticles, *Atmos. Res.*, 90, 132–150, <https://doi.org/10.1016/j.atmosres.2008.01.005>, 2008.
- 510 Kulmala, M., Petäjä, T., Nieminen, T., Sipilä, M., Manninen, H. E., Lehtipalo, K., Dal, Maso, M., Aalto, P., Junninen, H., Paasonen, P., Riipinen, I., Lehtinen, K. E. J., Laaksonen, A., and Kerminen, V.-M.: Measurement of the nucleation of atmospheric aerosol particles, *Nat. Protocol.*, 7, 1651–1667, <https://doi.org/10.1038/nprot.2012.091>, 2012.
- Leaitch, W. R., Strapp, J. W., and Isaac, G. A.: Cloud droplet nucleation and cloud scavenging of aerosol sulphate in polluted atmospheres, *Tellus*, 38B, 328–344, <https://doi.org/10.1111/j.1600-0889.1986.tb00258.x>, 1986
- Leino, K., Nieminen, T., Manninen, H. E., Petäjä, T., Kerminen, V. M., and Kulmala, M.: Intermediate ions as a strong  
515 indicator of new particle formation bursts in a boreal forest, *Boreal Environ. Res.*, 21, 274–286, 2016.
- Li Y., Zhang F., Li Z., Sun L., Wang Z., Li P., Sun Y., Ren J., Wang Y. and Cribb M.: Influences of aerosol physiochemical properties and new particle formation on CCN activity from observation at a suburban site of China, *Atmos. Res.*, 188, 80–89, <https://doi.org/10.1016/j.atmosres.2017.01.009>, 2017.
- Li, Z., Niu, F., Fan, J. et al. Long-term impacts of aerosols on the vertical development of clouds and precipitation.  
520 *Nature Geosci* 4, 888–894, <https://doi.org/10.1038/ngeo1313>, 2011.
- Li, Z., Guo, J., Ding, A., Liao, H., Liu, J., Sun, Y., Wang, T., Xue, H., Zhang, H., and Zhu, B.: Aerosols and boundary-layer interactions and impact on air quality. *Natl. Sci. Rev.*, 4, 810–833, <https://doi.org/10.1093/nsr/nwx117>, 2017.
- Liu, C., Wang, T., Rosenfeld, D., Zhu, Y., Yue, Z., Yu, X.: Anthropogenic effects on cloud condensation nuclei  
525 distribution and rain initiation in East Asia. *Geophysical Research Letters*, 47, <https://doi.org/10.1029/2019GL086184>, 2019.
- Liu, J., Zhang, F., Xu, W., Sun, Y., Chen, L., Li, S.: Hygroscopicity of organic aerosols linked to formation mechanisms. *Geophysical Research Letters*, 48, <https://doi.org/10.1029/2020GL091683>, 2021.
- Ma, N., Zhao, C., Tao, J., Wu, Z., Kecorius, S., Wang, Z., Größ, J., Liu, H., Bian, Y., Kuang, Y., Teich, M., Spindler, G.,  
530 Müller, K., van Pinxteren, D., Herrmann, H., Hu, M., and Wiedensohler, A.: Variation of CCN activity during new particle formation events in the North China Plain, *Atmos. Chem. Phys.*, 16, 8593–8607, <https://doi.org/10.5194/acp-16-8593-2016>, 2016.
- Martin, G., Johnson, D.: The measurement and parameterization of effective radius of droplets in warm stratocumulus clouds.[J]. *Journal of the Atmospheric Sciences*, [https://doi.org/10.1175/1520-0469\(1994\)051<182](https://doi.org/10.1175/1520-0469(1994)051<182)  
535 3: TMAPOE>2.0.CO;2, 1994.

- Merikanto, J., Spracklen, D. V., Pringle, K. J., and Carslaw, K. S.: Effects of boundary layer particle formation on cloud droplet number and changes in cloud albedo from 1850 to 2000, *Atmos. Chem. Phys.*, 10, 695–705, <https://doi.org/10.5194/acp-10-695-2010>, 2010.
- Meskhidze, N., Nenes, A., Conant, W., Seinfeld, J.: Evaluation of a new cloud droplet activation parameterization with in situ data from CRYSTAL-FACE and CSTRIFE, *J. Geophys. Res.*, 110, D16202, <https://doi.org/10.1029/2004JD005703>, 2005.
- Morales, R. and Nenes, A.: Characteristic updrafts for computing distribution-averaged cloud droplet number and stratocumulus cloud properties, *J. Geophys. Res.*, 115, D18220, <https://doi.org/10.1029/2009JD013233>, 2010.
- Morales, R., Nenes, A.: Understanding the contributions of aerosol properties and parameterization discrepancies to droplet number variability in a global climate model. *Atmos Chem Phys* 14(9):4809–4826, 2014.
- Nenes, A., Chan, S., Abdul-Razzak, H., Chuang, P., and Seinfeld, J. H.: Kinetic limitations on cloud droplet formation and impact on cloud albedo, *Tellus* 53B, 133–149, <https://doi.org/10.3402/tellusb.v53i2.16569>, 2001.
- Nenes, A. and Seinfeld, J. H.: Parameterization of cloud droplet formation in global climate models, *J. Geophys. Res.*, 108, 4415, <https://doi.org/10.1029/2002JD002911>, 2003.
- Ng, N. L., Herndon, S. C., Trimborn, A., Canagaratna, M. R., Croteau, P. L., Onasch, T. B.: An aerosol chemical speciation monitor (ACSM) for routine monitoring of the composition and mass concentrations of ambient aerosol, *Aerosol Science and Tech*, 45(7): 780-794, <https://doi.org/10.1080/02786826.2011.560211>, 2011.
- Paasonen, P. and Tapper, U.: Positive matrix factorization: A nonnegative factor model with optimal utilization of error-estimates of data values, *Journal Citation Reports*, 5: 112-126, 10.1002/env.3170050203, 1994.
- Paasonen, P., Peltola, M., Kontkanen, J., Junninen, H., Kerminen, V.-M., and Kulmala, M.: Comprehensive analysis of particle growth rates from nucleation mode to cloud condensation nuclei in boreal forest, *Atmos. Chem. Phys.*, 18, 12085–12103, <https://doi.org/10.5194/acp-18-12085-2018>, 2018.
- Peng, J. F., Hu, M., Wang, Z. B., Huang, X. F., Kumar, P., Wu, Z. J., Guo, S., Yue, D. L., Shang, D. J., Zheng, Z., and He, L. Y.: Submicron aerosols at thirteen diversified sites in China: size distribution, new particle formation and corresponding contribution to cloud condensation nuclei production, *Atmos. Chem. Phys.*, 14, 10249–10265, <https://doi.org/10.5194/acp-14-10249-2014>, 2014.
- Peng, Y., Dong, Y., Li, X. M.: Different Characteristics of New Particle Formation Events at Two Suburban Sites in Northern China. *Atmosphere*, 8(12), 258, <https://doi.org/10.3390/atmos8120258>, 2017.
- Petters, M. D. and Kreidenweis, S. M.: A single parameter representation of hygroscopic growth and cloud condensation



- 565 nucleus activity, *Atmos. Chem. Phys.*, 7, 1961–1971, <https://doi.org/10.5194/acp-7-1961-2007>, 2007.
- Ramanathan, V., Crutzen, P. J., Kiehl, J. T., and Rosenfeld, D.: Aerosols, climate, and the hydrological cycle, *Science*, 294, 2119–2124, <https://doi.org/10.1126/science.1064034>, 2001.
- Ren, J., Zhang, F., Wang, Y., Collins, D., Fan, X., Jin, X., Xu, W., Sun, Y., Cribb, M., and Li, Z.: Using different assumptions of aerosol mixing state and chemical composition to predict CCN concentrations based on field  
570 measurements in urban Beijing, *Atmos. Chem. Phys.*, 18, 6907–6921, <https://doi.org/10.5194/acp-18-6907-2018>, 2018.
- Rose, C., Sellegri, K., Moreno, I., Velarde, F., Ramonet, M., Weinhold, K., Krejci, R., Andrade, M., Wiedensohler, A., Ginot, P., and Laj, P.: CCN production by new particle formation in the free troposphere, *Atmos. Chem. Phys.*, 17, 1529–1541, <https://doi.org/10.5194/acp-17-1529-2017>, 2017.
- Seinfeld, J. H., Bretherton, C. S., Carslaw, K. S., Coe, H., DeMott, P. J., Dunlea, E. J., Feingold, G., Ghan, S. J., Guenther, A.B., Kahn, R. A., Kracunas, I. P., Kreidenweis, S. M., Molina, M. J., Nenes, A., Penner, J. E., Prather, K. A.,  
575 Ramanathan, V., Ramaswamy, V., Rasch, P. J., Ravishankara, A. R., Rosenfeld, D., Stephens, G., and Wood R.: Improving Our Fundamental Understanding of the Role of Aerosol-Cloud Interactions in the Climate System, *P. Nat. Acad. Sci. USA*, 113, 5781–5790, <https://doi.org/10.1073/pnas.1514043113>, 2016.
- Shi, J., Khan, A., Harrison, R.: Measurements of ultrafine particle concentration and size distribution in the urban  
580 atmosphere, *Science of the Total Environment*, 235(1-3):51-64, [https://doi.org/10.1016/S0048-9697\(99\)00189-8](https://doi.org/10.1016/S0048-9697(99)00189-8), 1999.
- Spracklen, D. V., Carslaw, K. S., Merikanto, J., Mann, G. W., Reddington, C. L., Pickering, S., Ogren, J. A., Andrews, E., Baltensperger, U., Weingartner, E., Boy, M., Kulmala, M., Laakso, L., Lihavainen, H., Kivekäs, N., Komppula, M., Mihalopoulos, N., Kouvarakis, G., Jennings, S. G., O'Dowd, C., Birmili, W., Wiedensohler, A., Weller, R., Gras, J., Laj, P., Sellegri, K., Bonn, B., Krejci, R., Laaksonen, A., Hamed, A., Minikin, A., Harrison, R. M., Talbot, R., and Sun, J.:  
585 Explaining global surface aerosol number concentrations in terms of primary emissions and particle formation, *Atmos. Chem. Phys.*, 10, 4775–4793, <https://doi.org/10.5194/acp-10-4775-2010>, 2010.
- Stanier, C., Khlystov, A., Pandis, S.: Ambient aerosol size distributions and number concentrations measured during the Pittsburgh Air Quality Study (PAQS), *Atmospheric Environment*, 38(20):3275-3284, <https://doi.org/10.1016/j.atmosenv.2004.03.020>, 2004.
- 590 Sullivan, S. C., Lee, D., Oreopoulos, L., and Nenes, A.: The role of updraft velocity in temporal variability of cloud hydrometeor number, *P. Natl. Acad. Sci. USA*, 113, 5781–5790, <https://doi.org/10.1073/pnas.1514043113>, 2016.
- Sun, Y. L., Wang, Z. F., Du, W., Zhang, Q., Wang, Q. Q., Fu, P. Q., Pan, X. L., Li, J., Jayne, J., and Worsnop, D. R.: Longterm real-time measurements of aerosol particle composition in Beijing, China: seasonal variations,

- meteorological effects, and source analysis, *Atmos. Chem. Phys.*, 15, 10149–10165,  
595 <https://doi.org/10.5194/acp-15-10149-2015>, 2015.
- Tao, J., Kuang, Y., Ma, N., Hong, J., Sun, Y., Xu, W., Zhang, Y., He, Y., Luo, Q., Xie, L., Su, H., and Cheng, Y.:  
Secondary aerosol formation alters CCN activity in the North China Plain, *Atmos. Chem. Phys.*, 21, 7409–7427,  
<https://doi.org/10.5194/acp-21-7409-2021>, 2021.
- Topping, D. O., McFiggans, G. B., and Coe, H.: A curved multi-component aerosol hygroscopicity model framework:  
600 Part 1 - Inorganic compounds, *Atmos. Chem. Phys.*, 5, 1205–1222, <https://doi.org/10.5194/acp-5-1205-2005>, 2005.
- Twomey, S.: The influence of pollution on the shortwave albedo of clouds, *J. Atmos. Sci.*, 34, 1149–1152,  
10.1175/1520-0469(1977)0342.0.CO;2, 1977.
- Wang, S. C. and Flagan, R. C.: Scanning Electrical Mobility Spectrometer, *Aerosol Sci. Tech.*, 13, 230–240,  
10.1080/02786829008959441, 1990.
- 605 Wang Y., Zhang F., Li Z., Tan H., Xu H., Ren J., Zhao J., Du W. and Sun Y.: Enhanced hydrophobicity and volatility of  
submicron aerosols under severe emission control conditions in Beijing, *Atmos Chem Phys*, 17, 5239–5251,  
<https://doi.org/10.5194/acp-17-5239-2017>, 2017.
- Wiedensohler, A., Birmili, W., Nowak, A., Sonntag, A., Weinhold, K., Merkel, M., Wehner, B., Tuch, T., Pfeifer, S.:  
Mobility particle size spectrometers: harmonization of technical standards and data structure to facilitate high quality  
610 long-term observations of atmospheric particle number size distributions, *Atmos. Meas. Tech.*, 5, 657–685,  
<https://doi.org/10.5194/amt-5-657-2012>, 2012.
- Wiedensohler, A., Chen, Y. F., Nowak, A., Wehner, B., Achtert, P., Berghof, M., Birmili, W., Wu, Z. J., Hu, M., Zhu, T.,  
Takegawa, N., Kita, K., Kondo, Y., Lou, S. R., Hofzumahaus, A., Holland, F., Wahner, A., Gunthe, S. S., Rose, D., Su,  
H., and Pöschl, U.: Rapid aerosol particle growth and increase of cloud condensation nucleus activity by secondary  
615 aerosol formation and condensation: A case study for regional air pollution in northeastern China, *J. Geophys. Res.*,  
114, D00G08, <https://doi.org/10.1029/2008JD010884>, 2008.
- Wu, Z., Hu, M., Liu, S., Wehner, B., and Wiedensohler, A.: Particle number size distribution in the urban atmosphere of  
Beijing, China, *Atmos. Environ.*, 42, 7967–7980, <https://doi.org/10.1016/j.atmosenv.2008.06.022>, 2008.
- Wu, Z. J., Hu, M., Yue, D. L.: Evolution of particle number size distribution in an urban atmosphere during episodes of  
620 heavy pollution and new particle formation. *Sci China Earth Sci*, 2011, 54, <https://doi.org/10.1007/s11430-011-4227-9>,  
2011.
- Wu, Z. J., Poulain, L., Birmili, W., Größ, J., Niedermeier, N., Wang, Z. B., Herrmann, H., and Wiedensohler, A.: Some

- insights into the condensing vapors driving new particle growth to CCN sizes on the basis of hygroscopicity measurements, *Atmos. Chem. Phys.*, 15, 13071–13083, <https://doi.org/10.5194/acp-15-13071-2015>, 2015.
- 625 Xu, W. Q., Han, T. T., Du, W., Wang, Q. Q., Chen, C., Zhao, J.: Effects of aqueous-phase and photochemical processing on secondary organic aerosol formation and evolution in Beijing, China. *Environmental Science & Technology*, 51(2), 762–770. <https://doi.org/10.1021/acs.est.6b04498>, 2017.
- Yue, D. L., Hu, M., Zhang, R. Y., Wu, Z. J., Su, H., Wang, Z. B., Peng, J. F., He, L. Y., Huang, X. F., Gong, Y. G., Wiedensohler, A.: Potential contribution of new particle formation to cloud condensation nuclei in Beijing[J].  
630 *Atmospheric Environment*, 45(33):6070-6077, <https://doi.org/10.1016/j.atmosenv.2011.07.037>, 2011.
- Zimmerman, A. , Petters, M. D. , & Meskhidze, N.: Observations of new particle formation, modal growth rates, and direct emissions of sub-10 nm particles in an urban environment. *Atmospheric Environment*, 242, 117835, 10.1016/j.atmosenv.2020.117835, 2020.
- Zhang, Q., Jimenez, J. L., Canagaratna, M. R., Ulbrich, I. M., Ng, N. L., Worsnop, D. R., and Sun, Y. L.: Understanding  
635 atmospheric organic aerosols via factor analysis of aerosol mass spectrometry: A review. *Analytical and Bioanalytical Chemistry*, 401(10), 3045–3067. <https://doi.org/10.1007/s00216-011-5355-y>, 2011.
- Zhang, F., Li, Y., Li, Z., Sun, L., Li, R., Zhao, C., Wang, P., Sun, Y., Liu, X., Li, J., Li, P., Ren, G., and Fan, T.: Aerosol hygroscopicity and cloud condensation nuclei activity during the AC3Exp campaign: implications for cloud condensation nuclei parameterization, *Atmos. Chem. Phys.*, 14, 13423–13437,  
640 <https://doi.org/10.5194/acp-14-13423-2014>, 2014.
- Zhang, F., Li, Z., Li, Y., Sun, Y., Wang, Z., Li, P., Sun, L., Wang, P., Cribb, M., Zhao, C., Fan, T., Yang, X., and Wang, Q.: Impacts of organic aerosols and its oxidation level on CCN activity from measurement at a suburban site in China, *Atmos. Chem. Phys.*, 16, 5413–5425, <https://doi.org/10.5194/acp-16-5413-2016>, 2016.
- Zhang, F., Wang, Y., Peng, J., Ren, J., Collins, D., Zhang, R., Li, Z.: Uncertainty in predicting CCN activity of aged and  
645 primary aerosols. *Journal of Geophysical Research: Atmospheres*, 122, 11,723–11,736. <https://doi.org/10.1002/2017JD027058>, 2017.
- Zhang, F., Ren, J., Fan, T., Chen, L., Xu, W., Sun, Y.: Significantly enhanced aerosol CCN activity and number concentrations by nucleation - initiated haze events: A case study in urban Beijing. *J. Geophys. Res.-Atmos.*, 124. <https://doi.org/10.1029/2019JD031457>, 2019.
- 650 Zheng, Y. T., Rosenfeld, D., Li, Z. Q.: Satellite Inference of Thermals and Cloud-Base Updraft Speeds Based on Retrieved Surface and Cloud-Base Temperatures, *Journal of the Atmospheric Sciences*, 2015, 72(6),

<https://doi.org/10.1175/JAS-D-14-0283.1,2015>.